Robust GNSS receivers by array signal processing: Theory and implementation

Carles Fernández–Prades, *Senior Member, IEEE,* Javier Arribas, *Senior Member, IEEE,* and Pau Closas, *Senior Member, IEEE.*

***Abstract*—One of the main vulnerabilities of GNSS receivers is their exposure to intentional or unintentional jamming signals, which could even cause service unavailability. Several alternatives to counteract these effects were proposed in the literature, being the most promising those based on multiple antenna architectures. This is specially the case for high-grade receivers used in applications requiring reliability and robustness. This article provides an overview of the possible receiver architectures encompassing antenna arrays and the associated signal processing techniques. Emphasis is also put on the most typical implementation issues found when dealing with such technology. A thorough survey is complemented with a set of experiments, including real data processing by a working prototype, which exemplifies the above ideas.**

***Index Terms*—Radio navigation; Satellite navigation systems; Global Positioning System; Adaptive arrays; Array signal processing; Receiving antennas; Robustness; Electromagnetic interference; Availability.**

I. Introduction

GLOBAL Navigation Satellite Systems (GNSS) offer a worldwide service thanks to a network of dedicated satellites. While in indoor scenarios plenty of technologies are available [1], GNSS are recognized to be the systems of choice in outdoor environments and, to a great extent, one of the most accurate source of position (and precise timing) information when it is available. Societal dependance on GNSS technology is increasing over the years and, nowadays, many industrial sectors are, in some sense, GNSS-driven. Therefore, GNSS vulnerabilities constitute a major concern for its further deployment and penetration in new markets.

It is well known that sources of accuracy degradation due to atmospheric effects can be effectively mitigated by differential systems, even with long baselines [2]. However, interferences and multipath remain as potential causes of downgraded performance in GNSS receivers. While multipath can cause biases in the position, velocity and time (PVT) solution, interferences are one of the most jeopardizing sources of accuracy and reliability degradation, and even denial–of–service, of GNSS receivers [3], [4].

Typically, interferences are classified into *i*) *continuous waves*: narrowband signals generated by ultra high frequency (UHF) and very high frequency (VHF) television broadcasting [5], [6], by some VHF omni–directional radio–range (VOR), and instrument landing system (ILS) harmonics [7], by spurious signals caused by power amplifiers working in the non–linearity region [8], or by oscillators present in many electronic devices such as personal computers and mobile phones, *ii*) *pulsed*, for instance those caused by distance measurement equipment (DME) and tactical air navigation system (TACAN) [9], both emitting pulsed modulations at the frequencies in the range 962–1213 MHz, which include the Galileo E5 and GPS L5 bands [10], or by wind profile radars (WPR) which operate on the band 1270–1295 MHz [11], close to the GPS L2C, GLONASS L2, and Galileo E6 bands; *iii*) *swept interferences*: signals characterized by a narrow instantaneous band at a central frequency that changes over time, usually harmonics of frequency modulated signals, which can be produced by telecommunication systems such as television and radio broadcasting, and *iv*) *wideband interferences*, understood as signals occupying most of the frequency band of interest. Basically, interferences affect the operation of the low noise amplifier (LNA) and the automatic gain control (AGC) of the RF front–end, and consequently have an impact in the performance of the carrier and code tracking loops, which results in deterioration of observables or even in complete loss of lock, thus turning into a disruptive event in the operation of a GNSS receiver. Analyses of RF interference effects in GNSS receivers can be found in [12] and [13], and real-life events were reported in [14], [15],

Interferences could also be intentional, like military jamming or hijackers using GPS jammers to prevent a stolen vehicle from being tracked. In addition, it is possible to build a transmitter of signals nearly identical to those sent by a satellite, with the objective of forging counterfeit navigation messages, or biasing the synchronization parameter estimations, transmitting them over an area containing one or more receivers, thus manipulating their PVT solutions. These techniques are known as *spoofing*, when the attacker synthesizes its transmissions, or *meaconing*, when (parts of) legitimate GNSS transmissions are re–used. Spoofing effects have been described and analyzed in [16]–[21].

Aside from (or in combination with) time–frequency countermeasures [22]–[24] and receiver autonomous integrity monitoring (RAIM) consistency checks [25], which are proved to be effective against continuous wave interferences, the spatial diversity provided by a set of antenna elements enables a powerful tool for interference mitigation. From the vast literature available on antenna arrays, a few percentage of works address the particularities of GNSS receivers. For instance, in most wireless communications applications multipath can be

Authors are with the Statistical Inference for Communications and Positioning Department, Communication Systems Division, Centre Tecnològic de Telecomunicacions de Catalunya (CTTC), Castelldefels, 08860 Barcelona, Spain. e-mail: {cfernandez,jarribas,pclosas}@cttc.cat

Manuscript submitted on March 10, 2017.

exploited to increase the signal–to–noise ratio and thus reduce the bit error rate. This is not the main issue in GNSS so far due to its low data rate and high processing gain. On the contrary, close multipath causes a bias in time–delay estimation and, thus, in position. Another example can be found in temporal–reference based beamformers, which exploit a training sequence in order to identify and synchronize the desired waveform; in GNSS the designer is not interested in the received waveform since desired signals are received well below the noise floor. Therefore, application of antenna arrays to GNSS receivers should be carefully designed considering that it is not a mere adaptation from wireless communication systems' concepts. Examples of works specifically devoted to GNSS particularities can be found in [26]–[38]. The specific problem of precise GNSS positioning using antenna arrays has been addressed in [39], [40].

This paper explores multi-antenna architectures and techniques specifically addressed to GNSS signals, which are direct–sequence spread–spectrum modulations received well below the noise floor, and where only the line–of–sight (LOS) propagation path contains useful information, that is, distance from the satellite to the navigation receiver. The objective is the minimization of interferences and multipath effects, ultimately enhancing the availability, accuracy and reliability of GNSS receivers.

II. Signal model

This section presents a generic model for GNSS signals, their respective multipath reflections, possible interferences and noise received at an antenna array. The notation is as follows: lowercase italics for scalar variables, either deterministic or stochastic, both real or complex; uppercase italics for constants; lowercase bold for vector variables, column–wise defined; uppercase bold for matrix variables; $(\cdot)^\top$, $(\cdot)^*$, and $(\cdot)^H$ stand for the transpose, conjugate, and conjugate transpose (hermitic) operators, respectively; and $\mathbb{E}\{\cdot\}$ is the expected value operator. More notation will be defined throughout the paper as needed.

An N–element antenna array receives signals from M satellites, each one with $M(m)$ scaled, time–delayed and Doppler–shifted replicas (multipath), plus interferences and thermal noise. At each antenna, the receiving baseband signal can be modeled as

$$x(t)=\sum_{m=1}^{M}\sum_{p=0}^{M(m)-1} a_{m,p}s_m(t-\tau_{m,p})e^{j2\pi f_{m,p}t}+\sum_{\ell=1}^{M_I} i_\ell(t)+n(t)\ , \tag{1}$$

where $\tau_{m,p}$ is the delay, $f_{m,p}$ is the Doppler shift for $p = 0, ..., M(m)-1$ received replicas of the m-th satellite signal (the LOS signal is denoted by the subindex $p = 0$), $i_\ell(t)$, $\ell = 1, ..., M_I$ are uncorrelated interferences, and $n(t)$ is additive white Gaussian noise. Each antenna receives a different replica of those signals, with a different phase depending on the array geometry and the direction of arrival (DOA). This can be expressed by a vector signal model, where each row corresponds to one antenna:

$$\mathbf{x}(t)=\sum_{m=1}^{M}\mathbf{H}_m\mathbf{b}_m(t)+\mathbf{H}_I\mathbf{i}(t)+\mathbf{n}(t)\ , \tag{2}$$

where:

- $\mathbf{x}(t)\in\mathbb{C}^{N\times 1}$ is the observed signal vector (snapshot),
- $\mathbf{H}_m\in\mathbb{C}^{N\times M(m)}$ is the spatial signature matrix related to array geometry and DOAs of the desired satellite signal m and its corresponding $M(m)$ echoes,
- $\mathbf{b}_m(t)=\begin{bmatrix} a_{m,0}s_m(t-\tau_{m,0})e^{j2\pi f_{m,0}t} \\ \vdots \\ a_{m,M(m)-1}s_m(t-\tau_{m,M(m)-1})e^{j2\pi f_{m,M(m)-1}t}\end{bmatrix}$ $\in\mathbb{C}^{M(m)\times 1}$ is the delayed and Doppler–shifted satellite signals envelopes vector, as received in the phase center of the antenna array,
- $\mathbf{H}_I\in\mathbb{C}^{N\times M_I}$ is the spatial signature matrix related to array geometry and DOAs of the interferences,
- $\mathbf{i}(t)\in\mathbb{C}^{M_I\times 1}$ are the uncorrelated interferences, as received in the phase center of the antenna array, and
- $\mathbf{n}(t)\in\mathbb{C}^{N\times 1}$ represents additive white Gaussian noise received at each antenna.

The spatial signature matrix $\mathbf{H}$ can be expressed as a function of the scenario geometry and the electrical characteristics of the antenna array:

$$\mathbf{H}=\mathbf{C}\mathbf{G}\ . \tag{3}$$

Matrix $\mathbf{C}\in\mathbb{C}^{N\times N}$ models RF channels' gain and phase unalignments, as well as cross-coupled terms, which can be measured in a calibration process. On the other hand, matrix $\mathbf{G}\in\mathbb{C}^{N\times M}$ depends on the geometry of the array and on the position of the sources or considered scatterers, and it is uniquely defined for a set of sources emitting from different directions. Considering a local coordinate system (for example, an east–north–up or $[e, n, u]$ system with origin in a reference point, usually the phase center of the whole array), the delay between the array antenna elements $\Delta t_{m,n}$, where m refers to a given source and n refers to a given antenna, can be computed as the dot product of the wave vector $\mathbf{k}_m$ (with modulus $\frac{2\pi}{\lambda_m}$, being λ_m the carrier wavelength of signal m and its direction pointing to the signal source, defined by its azimuth ϕ_m and elevation θ_m) and the position of the antenna center of phase, $\mathbf{r}_n$. Generalizing this example for M sources and N antennas with arbitrary geometry, the time delay of each source caused in each antenna can be computed and expressed in a matrix form

$$\mathbf{G}=e^{j\pi(\mathbf{K}\mathbf{R})^\top}\ , \tag{4}$$

where $\mathbf{K}\in\mathbb{R}^{M\times 3}$ is the wavenumber matrix, defined as

$$\mathbf{K}=\begin{pmatrix} \cos(\phi_1)\cos(\theta_1) & \sin(\phi_1)\cos(\phi_1) & \sin(\theta_1) \\ \vdots & \vdots & \vdots \\ \cos(\phi_M)\cos(\theta_M) & \sin(\phi_M)\cos(\theta_M) & \sin(\theta_M)\end{pmatrix}, \tag{5}$$

having its rows pointing towards the corresponding emitter, being ϕ_i the angle of the source i defined anticlockwise from

the e axis on the en plane and θ_i the angle with respect to the en plane. On the other hand,

$$\mathbf{R} = \begin{pmatrix} r_{e_1} & \dots & r_{e_N} \\ r_{n_1} & \dots & r_{n_N} \\ r_{u_1} & \dots & r_{u_N} \end{pmatrix} \qquad \in \mathbb{R}^{3\times N} \tag{6}$$

is the matrix of sensor element positions normalized to units of half wavelengths with respect to the e, n and u axes.

In this model, the *narrowband array assumption* has been made. This assumption considers that the time required for the signal to propagate along the array is much smaller than the inverse of its bandwidth and, thus, a phase shift can be used to describe the propagation from one antenna to another. For instance, for a navigation signal transmitted with a 20-MHz bandwidth, its inverse is 50 ns, or 15 m in spatial terms. The array is expected to be much smaller, since the carrier's half–wavelength is on the order of 10 cm, so the assumption seems reasonable. However, it must be pointed out that this signal model becomes invalid for large arrays. In the same way, it is assumed that the Doppler effect can be modeled by a frequency shift, which is commonly referred to as the *narrowband signal assumption* [41], [42]. Again, this is well justified because the bandwidth of the GNSS signals is on the order of few megahertz, and the carrier frequency is between 1 and 2 GHz.

GNSS signals $s_m(t)$, whose waveforms are known at the receiver, are transmitted using spread–spectrum techniques (see [43] for a description of GNSS civil signals), resulting in a received signal buried in noise. Therefore, a collection of K snapshots (usually spanning one or more spreading codeword periods) are used to take advantage of the despreading gain.

Suppose that K snapshots of the impinging signal are taken with a sampling interval T_s satisfying the Nyquist criterion. Then, the sampled data can be expressed as

$$\mathbf{X}[k] = \sum_{m=1}^{M} \mathbf{H}_m \mathbf{B}_m[k] + \mathbf{H}_I \mathbf{I}[k] + \mathbf{N}[k] \ , \tag{7}$$

using the following definitions:

- $\mathbf{X}[k] = \begin{pmatrix} \mathbf{x}(t_{k-K+1}) & \cdots & \mathbf{x}(t_k) \end{pmatrix} \in \mathbb{C}^{N\times K}$, referred to as the *spatiotemporal data matrix*, where we used $t_k \equiv kT_s$,
- $\mathbf{B}_m[k] = \begin{pmatrix} \mathbf{b}_m(t_{k-K+1}) & \cdots & \mathbf{b}_m(t_k) \end{pmatrix} \in \mathbb{C}^{M(m)\times K}$, known as basis function matrices,
- $\mathbf{I}[k] = \begin{pmatrix} \mathbf{i}(t_{k-K+1}) & \cdots & \mathbf{i}(t_k) \end{pmatrix} \in \mathbb{C}^{M_I\times K}$, known as the interference functions matrix, and
- $\mathbf{N}[k] = \begin{pmatrix} \mathbf{n}(t_{k-K+1}) & \cdots & \mathbf{n}(t_k) \end{pmatrix} \in \mathbb{C}^{N\times K}$.

The signal model in (7) admits a number of particularizations and statistical assumptions (for instance, interferences and multipath can be excluded, or considered random with a given probability density) leading to a plethora of possible receiver architectures and techniques for array signal processing. The next section summarizes the state-of-the-art.

III. Receiver Design and Architecture

Single-antenna receivers can implement a number of multipath and interference countermeasures, summarized in Figure 1. Basically, they consist of providing the receiver with a fixed reception pattern antenna (FRPA) with a radiation pattern attenuating signals coming from low elevation angles (for instance, a choke-ring antenna [44]), a larger input dynamic range in order to avoid saturation, some digital signal processing techniques addressing the presence of those undesired signals, as well as consistency checks.

However, those countermeasures could provide insufficient rejection capabilities in extremely challenging scenarios. A possible solution for providing enhanced robustness to the receiver is to resort to controlled reception pattern antennas (CRPAs), also known as adaptive antenna arrays, a technology that can provide up to 90 dB of jamming rejection depending on the specific architecture used [54]. Its main disadvantage is that it requires an array of antenna elements, each spaced half a wavelength apart (about 10 cm) from center to center, which means that those systems are physically large in the GNSS receiver context.

Generally speaking, a CRPA consists of several antenna elements whose outputs are controlled in phase and gain, *i.e.*, multiplied by complex weights and combined together in a single output, in order to achieve a gain pattern that can be manipulated electronically. Considering again an N–element array, the mentioned weights can be stacked in a complex–valued vector $\mathbf{w} \in \mathbb{C}^{N\times 1} = \begin{bmatrix} w_0 & \cdots & w_{N-1} \end{bmatrix}^\top$, and the output signal of a beamformer can be computed as $\mathbf{y} = \mathbf{w}^H\mathbf{X}$.

Two general types of CRPAs are used with GNSS receivers: single-output nulling antennas and multiple-output beamsteering antennas. Most deployed systems are single-output adaptive nulling antennas that operate as an antijamming appliqué. In this way, a GNSS receiver need not know the type of antenna it is connected to, be it FRPA or CRPA. However, research and development trends focus on multiple-output beamsteering architectures, in spite of requiring the development of a whole custom receiver that able to handle those multiple antenna outputs, due to its superior performance.

A. Single-output adaptive nullers

This type of antenna array is used to sense the presence of interfering signals and adaptively placing reception nulls in the direction of arrival of such signals. The general diagram of such architecture is shown in Figure 2, where the antenna array delivers a single output that can feed a *conventional* (*i.e.*, single antenna) receiver.

A simple example of beamweight design that can be found is the power minimization nuller $\hat{\mathbf{w}}_{\text{PMIN}}$ (see Table I, where $\hat{\mathbf{R}}_{\mathbf{XX}} = \frac{1}{K}\mathbf{X}\mathbf{X}^H$ is an estimation of the autocorrelation matrix of the received snapshots). This power minimization approach is founded on the fact that GNSS signals are received well below the noise floor (and can be recovered based on their corresponding spreading sequence), and thus they pass through the beamformer seamlessly. This architecture can steer up to $N-1$ nulls by adjusting a set of N control weights, since only one degree of freedom is consumed in constraining the reference element weight to be unity.

Other more sophisticated strategies are possible. For instance, the power minimization can be constrained to point to multiple directions (that is, to multiple satellites at the

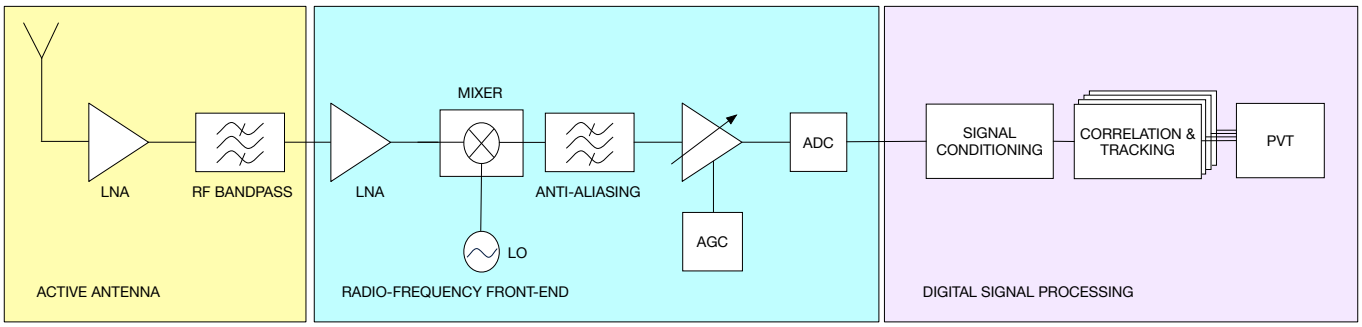

Fig. 1. Single-antenna GNSS receiver architectures can implement interference countermeasures at different levels: *Antenna* (*e.g.* appropriate reception pattern, sharp out-of-band filtering, high compression point of LNA), *RF front-end* (*e.g.* high dynamic range mixing [6], multi-level ADC [45], adaptive quantization levels [46], short relaxation time of AGC, interference detection [47]), and *digital signal processing* (*e.g.* digital pulse blanking [48], adaptive notch filter [49], robust design of tracking loops [50]–[52], inertial coupling, data fusion, network aiding [53]).

same time). This scheme, known as multiple constrained minimum variance nuller (denoted as $\hat{\mathbf{w}}_{MCMV}$ in Table I, where $\mathbf{H}_{LOS} = [\mathbf{h}_1 \cdots \mathbf{h}_M] \in \mathbb{C}^{N\times M}$ is a matrix whose columns contain the steering vectors to the GNSS satellites, and $\mathbf{h}_m \in \mathbb{C}^{N\times 1}$ refers to the first column vector of matrix $\mathbf{H}_m$, which corresponds to the line-of-sight spatial signature of the m-th satellite) is expected to provide better performance with respect to the simple power minimization algorithm, at the expense of a higher computational load, the need of the expected DOAs, and consuming degrees of freedom for the desired signals. Pointing to M satellites, this approach can place up to $N-M$ nulls. A similar approach can be performed taking the satellite waveform as the temporal reference, leading to the minimum mean square error nuller, defined as $\hat{\mathbf{w}}_{\text{MMSE}}$ in Table I, where vector $\hat{\mathbf{a}} = [\hat{a}_{1,0}, \cdots, \hat{a}_{M,0}]^\top \in \mathbb{C}^{M\times 1}$ stores the estimated complex amplitudes of the line of sight signals, $\hat{\mathbf{R}}_{\mathbf{XD}_{\text{LOS}}} = \frac{1}{K}\mathbf{X}\mathbf{D}_{\text{LOS}}^H$ is an estimation of the cross-correlation matrix, $\mathbf{D}_{\text{LOS}} = \left[\mathbf{d}_1^\top \cdots \mathbf{d}_M^\top\right]^\top \in \mathbb{C}^{M\times K}$ is a matrix containing K samples of the M waveforms locally generated at the receiver, parameterized by its respective time delays $\boldsymbol{\tau} = [\tau_{1,0}, \cdots \tau_{M,0}]$ and Doppler shifts $\mathbf{f}_d = [f_{d_{1,0}}, \cdots, f_{d_{M,0}}]$. Local replicas $\mathbf{d}_m = [d_m(t_{k-K+1}) \cdots d_m(t_k)] \in \mathbb{C}^{1\times K}$ are sampled, unfiltered and normalized versions of the waveform $s_m(t-\tau_{m,0})e^{j2\pi f_{m,0}t}$, corresponding to the LOS signal of the m-th satellite. The behavior of the temporal reference beamforming tends to combine constructively all the impinging signals in order to increase the contribution of the desired signals at the nuller output.

Further enhancements can be achieved by including tapped delay lines behind each antenna element. Additional weights are applied to the delayed signals, yielding a finite impulse response (FIR) filter, and the results are combined in the weighted sum. Such structure is known as space-time adaptive processor (STAP) [28], [55]–[58]. Stacking the output of the N antennas and their P delayed samples in a column vector $\mathbf{x}_{\text{STAP}} = [x_1(t_k)\cdots x_1(t_{k-P+1}), \cdots, x_N(t_k)\cdots x_N(t_{k-P+1})]^\top \in \mathbb{C}^{NP\times 1}$, where P is the number of FIR filter taps, and the filters coefficients in a column vector $\mathbf{w}_{\text{STAP}} = [w_{11}\cdots w_{1P}, w_{21}\cdots w_{2P}, \cdots w_{NP}]^\top \in \mathbb{C}^{NP\times 1}$, the output of the STAP can be expressed as $y = \mathbf{w}_{\text{STAP}}^H \mathbf{x}_{\text{STAP}}$, thus obtaining a signal model that admits the formulations and solutions of Table I. This approach achieves deeper nulls and better performance in the rejection of wideband interferers than using one weight per antenna element, at the expense of a higher computational load. In addition, those FIR filters' time taps may distort the spread-spectrum GNSS ranging signal, introducing biases that must be compensated [59].

As examples of deployed systems, it can be mentioned Raytheon's GPS anti-jamming products, known as GAS-1, MiniGAS, and Advanced Digital Antenna Production (ADAP) systems [60]. GAS-1 is a 7-element adaptable phased-array antenna, and ADAP adds enhanced interference mitigation and dual-frequency beamforming capabilities. Another example is NovAtel Inc. and QinetiQ Ltd.'s dual-frequency GPS Anti-Jam Antenna (GAJT) [61], which features 7 antenna elements creating up to 6 independent nulls in GPS L1 and L2. The size of this CRPA is a diameter of 29 cm and a height of 12 cm, weighting 7.5 kg.

B. Multiple-output adaptive beamformers

Instead of conforming nulls to reject interfering signals, the so-called multiple-output adaptive beamformers produce M independent beams, each one devoted to a given satellite and providing its corresponding output. The weighting vector $\mathbf{w}$, also known as *beamvector*, can be designed following several criteria, usually encompassed in two families – namely, time reference beamformers relying on *a priori* knowledge of a reference waveform, and spatial reference beamformers relying on *a priori* knowledge of the spatial signature of the desired DOA. A possible diagram of such architecture is shown in Figure 3.

Some examples of design criteria are provided in Table II, where $\mathbf{w}_m$ refers to the beamweight of the m-th beamformer, $\hat{\mathbf{r}}_{\mathbf{xd}_m} = \frac{1}{K}\mathbf{X}\mathbf{d}_m^H$ is an estimation of the cross-correlation vector between the received array snapshots and a satellite signal replica locally generated at the receiver, and $\mathcal{P}\{\cdot\}$ is the operator that yields the principal eigenvector of a matrix, *i.e.*, the eigenvector that corresponds to the maximal eigenvalue. A comprehensive review of possible algorithms for adaptive beamforming can be found in [68].

The algorithms described in Table II are all linear; therefore they can be applied either at the pre-correlation or at the post-

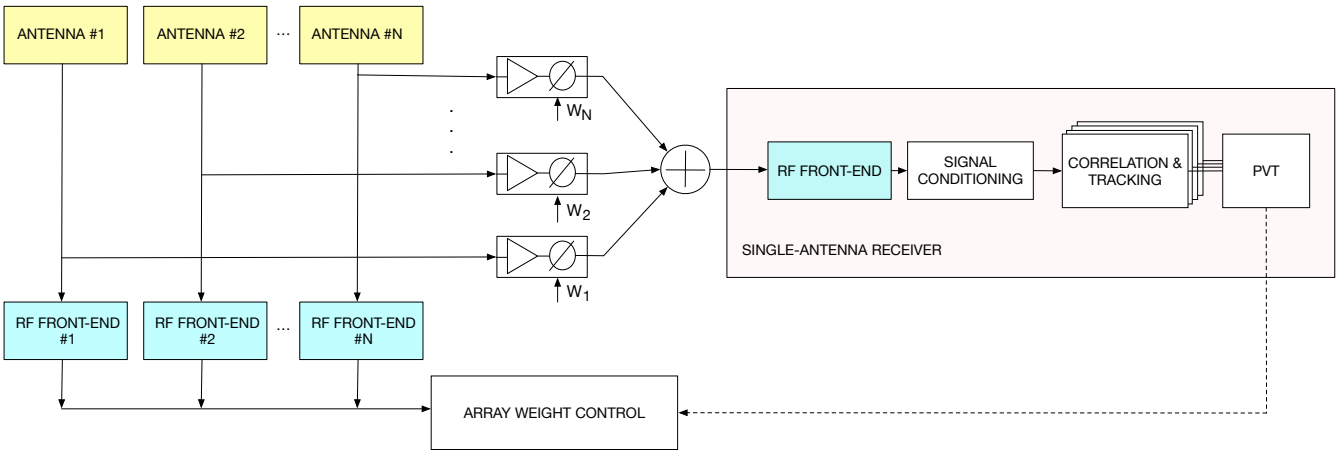

Fig. 2. Single-output adaptive nulling antenna architecture. This approach modifies gains and phases at RF level, using variable amplifiers and phase shifters and delivering a single, filtered output that can be plugged into any GNSS receiver, thus allowing the antenna array to operate as an antijamming appliqué. Beamweights can belong to some predefined sets or to be adaptively computed from the RF front-end outputs and possibly other information from the receiver.

TABLE I
EXAMPLES OF SINGLE-OUTPUT BEAMWEIGHT DESIGN.

Name	Criterion	Optimum beamweight	Requires	Refs.
Power minimization	$\arg\min_{\mathbf{w}} \mathbb{E}\left\{\left\|\mathbf{w}^H\mathbf{X}\right\|^2\right\}$ subject to $\mathbf{w}^H\boldsymbol{\delta}_0 = 1, \quad \boldsymbol{\delta}_0 = [1, 0, ..., 0]^\top$	$\hat{\mathbf{w}}_{\text{PMIN}} = \dfrac{\hat{\mathbf{R}}_{\mathbf{XX}}^{-1}\boldsymbol{\delta}_0}{\boldsymbol{\delta}_0^\top\hat{\mathbf{R}}_{\mathbf{XX}}^{-1}\boldsymbol{\delta}_0}$	$\mathbf{X}$	[30], [62] [63]–[65]
Multiple-Constrained Minimum Variance	$\arg\min_{\mathbf{w}} \mathbb{E}\left\{\left\|\mathbf{w}^H\mathbf{X}\right\|^2\right\}$ subject to $\mathbf{w}^H\mathbf{h}_m = 1, \quad m = 1, ..., M$	$\hat{\mathbf{w}}_{\text{MCMV}} = \dfrac{\hat{\mathbf{R}}_{\mathbf{XX}}^{-1}\hat{\mathbf{H}}_{\text{LOS}}}{\hat{\mathbf{H}}_{\text{LOS}}^H\hat{\mathbf{R}}_{\mathbf{XX}}^{-1}\hat{\mathbf{H}}_{\text{LOS}}}\mathbf{1}_{M\times 1}$	$\mathbf{X}$, $\hat{\mathbf{H}}_{\text{LOS}}$	[26], [55], [66]
Minimum Mean Square Error	$\arg\min_{\mathbf{w}} \mathbb{E}\left\{\left\|\mathbf{w}^H\mathbf{X} - \mathbf{a}^\top\mathbf{D}_{\text{LOS}}\right\|^2\right\}$	$\hat{\mathbf{w}}_{\text{MMSE}} = \hat{\mathbf{R}}_{\mathbf{XX}}^{-1}\hat{\mathbf{R}}_{\mathbf{XD}_{\text{LOS}}}\hat{\mathbf{a}}^*$	$\mathbf{X}$, $\hat{\mathbf{a}}$, $\mathbf{D}_{\text{LOS}}(\hat{\boldsymbol{\tau}}, \hat{\mathbf{f}}_d)$	[27], [67]

correlation level (see Figure 4), depending on the application and the available computational power, just by replacing the reference signals $\mathbf{d}_m$ by their despreaded versions and redefining the data matrix $\mathbf{X}$ to be at the output of the correlation banks. In general, interference detection and mitigation techniques are applied at the pre-correlation level, whereas multipath mitigation is performed at the post-correlation level where the data rate is much lower. Examples of reported implementations in which beamforming is performed after correlation can be found in [69]–[71].

The literature reports several digital beamforming implementations aimed at GNSS. One of the firstly reported commercial platforms was NAVSYS Corporation's High Gain Advanced GPS Receiver (HAGR) [72], which was composed of a 16-element antenna array receiver and used dedicated hardware to create up to 12 independent and parallel beamformings to simultaneously point the array beams towards 12 GPS satellites. Similar architectures were reported in [73]–[77], as well as combined with inertial navigation [78], [79] and attitude determination systems [80], [81].

C. Snapshot-based interference mitigation

Besides beamforming, another sort of array signal processing involves the joint processing of the N set of snapshots to estimate a set of desired quantities of interest. Within this context, interferences can also be mitigated by resorting to an algorithm based on the generalized likelihood ratio test (GLRT) detector [88] operating directly on the array snapshots, with no other prior knowledge than the satellites signals' waveforms. This is the case of a *cold start*, in which the receiver has no initial information of the potentially in-view satellites and needs to perform a signal acquisition stage in order to get the list of satellites actually in-view and initial estimations of their code phase and Doppler shift, a process known to suffer from the lowest sensitivity of the whole receiver operation and, consequently, becoming an availability bottleneck.

The GLRT detector takes into account the probability density function of $\mathbf{x}(t)$ to obtain a test statistic which is able to detect GNSS signals by maximizing the probability of detection subject to a given false alarm probability. The application of the GLRT to GNSS array-based receivers was derived and analyzed by the authors in [89], resulting in the following test statistics expression:

$$T_{GL}(\mathbf{X}) = \max_{f_d,\tau}\left\{\hat{\mathbf{r}}_{\mathbf{xd}}^H(f_d,\tau)\hat{\mathbf{R}}_{\mathbf{xx}}^{-1}\hat{\mathbf{r}}_{\mathbf{xd}}(f_d,\tau)\right\} \geq \gamma, \qquad (8)$$

where γ is the detection threshold. Equation (8) can be solved by an exhaustive grid search in the entire (f_d, τ) parameter

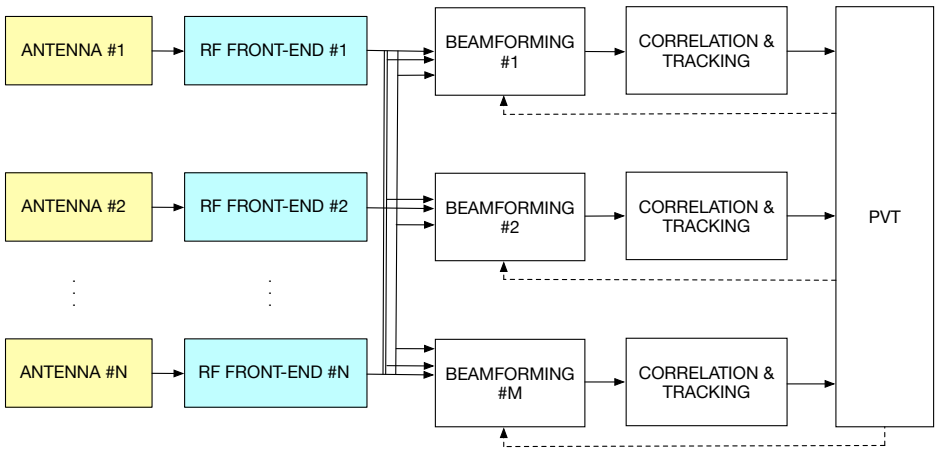

Fig. 3. Multiple-output adaptive beamsteering architecture. Software refined radio is a natural choice for the implementation of the custom GNSS receiver.

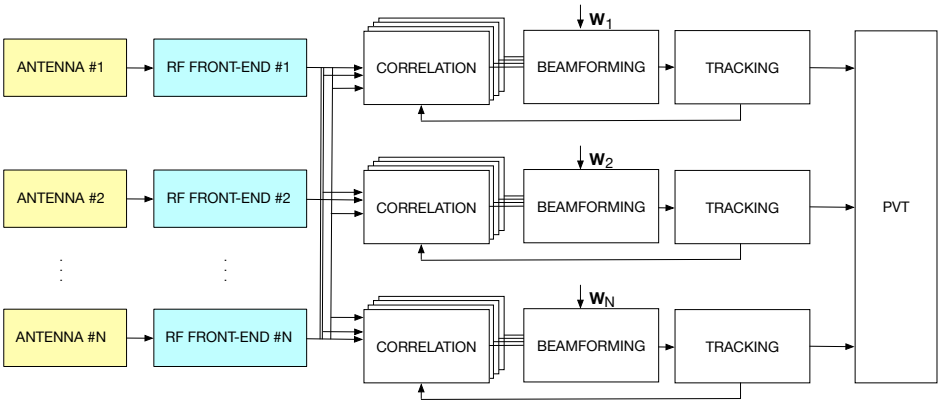

Fig. 4. Multiple-output beamsteering architecture after correlation. This scheme reduces drastically the computational requirements, since weight computation is performed on data after the despreading process.

space. The computational load of this process can be alleviated by resorting to the cross-correlation properties of the Fast Fourier Transform, which allows the parallelization of the code delay search for an specific Doppler frequency bin [90].

IV. Implementation Issues

The deployment of practical systems needs to face some implementation issues that may have an impact on the final performance. This section comments on the main concerns in their design.

A. Antenna phase center

The GNSS measurements are referred to the so-called antenna phase center (APC) position, defined as the apparent source of radiation. In an ideal antenna with spheric equiphase contour, such point would be fixed. Practical antenna implementations exhibit an irregular equiphase contour, causing the apparent APC to depend on the direction of arrival and signal frequency, with variations on the order of few millimiters. A point tied to the base of the antenna, named antenna reference point (ARP), is used as a more suitable reference. Since the adaptive beamforming will dynamically change the array pattern, it has the potential to introduce phase center biases into the antenna array. For applications demanding high accuracy, those phase biases must be mitigated or compensated because they will bring errors in the code and carrier phase measurements [91], [92]. Usually, antenna manufacturers provide technical information on the APC position relative to the ARP.

B. Calibration

Calibration of the antenna array implies the measurement of matrix $\mathbf{C}$ defined in Equation (3) and its compensation procedure, being the final objective to have the signature vectors $\mathbf{h}$ only parameterized by sources' azimuth and elevation. Measurements are usually performed in anechoic chambers with high degree of automatization, and phase compensations are performed in the digital domain with methods ranging from look-up tables to advanced adaptive algorithms acting as a preprocessor of the beamformer [81], [93]–[95]. Mutual coupling among elements was considered in, for instance, [96], [97]. A calibration strategy for STAP beamformers and an operational prototype was reported in [98]. Other examples include the use of an inertial measurement unit and live signals [99].

TABLE II
EXAMPLES OF MULTIPLE-OUTPUT BEAMWEIGHT DESIGN

Name	Criterion	Optimum beamweight	Requires	Refs.
Phased Array	$\mathbf{w}^H\mathbf{h}_m = 1$	$\hat{\mathbf{w}}_{\text{PAB}_m} = \hat{\mathbf{h}}_m \left(\hat{\mathbf{h}}_m^H \hat{\mathbf{h}}_m\right)^{-1}$	$\hat{\mathbf{h}}_m$	[82]–[84]
Linearly Constrained Minimum Variance	$\arg\min_{\mathbf{w}} \mathbb{E}\left\{\left\|\mathbf{w}^H\mathbf{X}\right\|^2\right\}$ subject to $\mathbf{w}^H\mathbf{h}_m = 1$	$\hat{\mathbf{w}}_{\text{MVB}_m} = \frac{\hat{\mathbf{R}}_{\mathbf{XX}}^{-1}\hat{\mathbf{h}}_m^H}{\hat{\mathbf{h}}_m\hat{\mathbf{R}}_{\mathbf{XX}}^{-1}\hat{\mathbf{h}}_m^H}$	$\mathbf{X}$, $\hat{\mathbf{h}}_m$	[74], [85]
Temporal Reference Beamformer	$\arg\min_{\mathbf{w}} \mathbb{E}\left\{\left\|\mathbf{w}^H\mathbf{X} - a_{m,0}\mathbf{d}_m\right\|^2\right\}$	$\hat{\mathbf{w}}_{\text{TRB}_m} = \hat{\mathbf{R}}_{\mathbf{XX}}^{-1}\hat{\mathbf{r}}_{\mathbf{Xd}_m}\hat{a}_{m,0}^*$	$\mathbf{X}$, $\hat{a}_{m,0}$ $\mathbf{d}_m\left(\hat{\tau}_{m,0}, \hat{f}_{d_{m,0}}\right)$	[86]
Hybrid Beamformer	$\arg\min_{\mathbf{w}} \mathbb{E}\left\{\left\|\mathbf{w}^H\mathbf{X} - a_{m,0}\mathbf{d}_m\right\|^2\right\}$ subject to $\mathbf{w}^H\mathbf{h}_m = 1$	$\hat{\mathbf{w}}_{\text{HB}_m} = \hat{\mathbf{w}}_{\text{TRB}_m} + \hat{\mathbf{w}}_{\text{MVB}_m}\left(1 - \hat{\mathbf{h}}_m^H\hat{\mathbf{w}}_{\text{TRB}_m}\right)$	$\mathbf{X}$, $\hat{\mathbf{h}}_m$, $\hat{a}_{m,0}$ $\mathbf{d}_m\left(\hat{\tau}_{m,0}, \hat{f}_{m,0}\right)$,	[31]
Eigenbeamforming	$\arg\min_{\mathbf{w}} \mathbb{E}\left\{\left\|\mathbf{w}^H\left(\mathbf{X} - \mathbf{h}_m^H a_{m,0}\mathbf{d}_m\right)\right\|^2\right\}$	$\hat{\mathbf{w}}_{\text{EIG}_m} = \mathcal{P}\left\{\frac{\left\|\hat{a}_{m,0}\right\|^2 \hat{\mathbf{h}}_m^H\hat{\mathbf{h}}_m + \hat{\sigma}_n^2\mathbf{I}_{N\times N}}{\hat{\mathbf{R}}_{\mathbf{XX}} - \left\|\hat{a}_{m,0}\right\|^2 \hat{\mathbf{h}}_m^H\hat{\mathbf{h}}_m}\right\}$	$\mathbf{X}$, $\hat{\mathbf{h}}_m$, $\left\|\hat{a}_{m,0}\right\|^2$, $\hat{\sigma}_n^2$	[87]

C. Practical implementation of adaptive schemes

Practical implementations of adaptive nullers and beamformers require online calculation of the covariance matrix inverse. However, this operation is computationally expensive because obtaining $\mathbf{X}[k]\mathbf{X}[k]^H$ requires a computation of order N^2K (where $K \geq \alpha \cdot 1023$, with $\alpha = 2$ in the simplest GPS L1 C/A case to $\alpha = 90$ for the wideband Galileo E5 signal), and its inverse is of order N^3. Furthermore, the numerical calculation of the weights in Tables I and II are known to be numerically unstable if the sample covariance matrix is ill-conditioned.

Both drawbacks can be alleviated by resorting to the QR decomposition-based recursive least squares algorithm [100], which allows the recursive computation of $(\mathbf{X}[k]\mathbf{X}[k]^H)^{-1}$ from $(\mathbf{X}[k-1]\mathbf{X}[k-1]^H)^{-1}$, requiring only computations of order N^2. This algorithm can be applied both to the spatially-constrained minimum variance and minimum mean square error approaches and, most importantly, it is well suited to very large scale integration (VLSI) implementation, as its orthogonal nature means that it is inherently well conditioned and can be implemented in a stable manner using relatively short word length arithmetic in FPGA devices [90], [101]–[104].

V. EXPERIMENTAL RESULTS

A. Numerical simulations

1) Signal acquisition performance: In order to assess the acquisition performance in realistic conditions, Galileo E1B and E1C Open Service signals were synthetically generated as described in [105]. For the numerical simulations, it was assumed a circular, $N = 8$ omnidirectional element antenna array, each element being half–wavelength apart from its neighbors, with their corresponding RF front–ends delivering a stream of complex samples at a sampling frequency of 6 Msps. The acquisition time was set to one PRN primary code period ($T_{acq} = 4$ ms, $K = 24000$ snapshots) and the probability of false alarm P_{fa} was set to 0.001 for all the algorithms in order to set the particular threshold values.

In all the experiments, $T_{\text{GL}}(\mathbf{X})$ stands for the array GLRT acquisition test statistics in Equation (8), $T_{\text{WH}}(\mathbf{X})$ is the same detector but assuming only white noise present in the antenna array ($\hat{\mathbf{R}}_{\mathbf{xx}} \simeq \mathbf{I}$), the blind null-steering attached to a conventional single-antenna acquisition is represented by $T_{\text{PMIN}}(\mathbf{X})$, the minimum variance nuller that uses satellite DOA estimations, also attached to a single-antenna acquisition, is represented as $T_{\text{MCMV}}(\mathbf{X})$. Finally, the array acquisition performance upper bound is given by $T_{\text{NP}}(\mathbf{X})$, as the Neymann-Pearson clairvoyant detector [106], provided as a reference performance bound.

In addition to the array-based acquisition algorithms, the tests included the performance of a single-antenna acquisition equipped with an interference remover based on a high-pass infinite impulse-response (IIR) notch, 5-tap Butterworth filter, tuned to remove the interference signal assuming a perfect estimation of its bandwidth. It is represented by $T_{\text{IIRNotch}}(\mathbf{x})$ in the figures. Figure 5 shows the probability of detection P_d for different carrier-to-noise density ratio (C/N_0) values in a scenario where a 500 kHz, Gaussian noise-like in-band interference impinges into a $N = 8$ elements array, with uniformly distributed random DOA and interference-to-noise density ratio $J/N_0 = 80$ dB-Hz. The simulated array was circular with uniformly separated elements at $\frac{\lambda}{2}$, and without a central element. λ was set to the Galileo E1 carrier wavelength. In addition, different pointing errors in the DOA estimation for the MCMV nuller were considered in order to simulate a moderately uncalibrated array. The error in DOA estimation was modeled as a Gaussian additive error term with different mean values ($\mu_e = 10^\circ$, $\mu_e = 15^\circ$, and $\mu_e = 20^\circ$) in both azimuth and elevation angles, and $\sigma_e^2 = 5^\circ$ of variance in all the cases.

The performance shown by the MCMV nuller reached almost the theoretical bound, but it is quite sensible to the accuracy of the DOA estimations and the array calibration. The GLRT array acquisition algorithm losses less than 3 dB of sensitivity with respect to the MCMV, and does not require any prior information. As expected, the power minimization filter losses about $10\log(N) \simeq 9$ dB less than the upper bound

due to the fact that it does not have any array gain towards the satellite signal DOA. Finally, the IIR notch filter performs about 13 dB below the upper bound as the frequency excision also removes a large portion of the satellite signal.

Figure 6 shows the results for the probability of detection vs. the interference bandwidth for the same set of algorithms, assuming a constant satellite $C/N_0 = 42$ dB-Hz and a constant wave interference with $J/N_0 = 80$ dB-Hz. As the interference bandwidth increases, the time and frequency protections lose the required diversity to discriminate between the satellite signal and the interferer. As expected, the IIR notch protection fail when the frequency excision is overlapped by the satellite signal spectrum. All the space-diversity protections are insensible to this test, obtaining a constant $P_d = 1$.

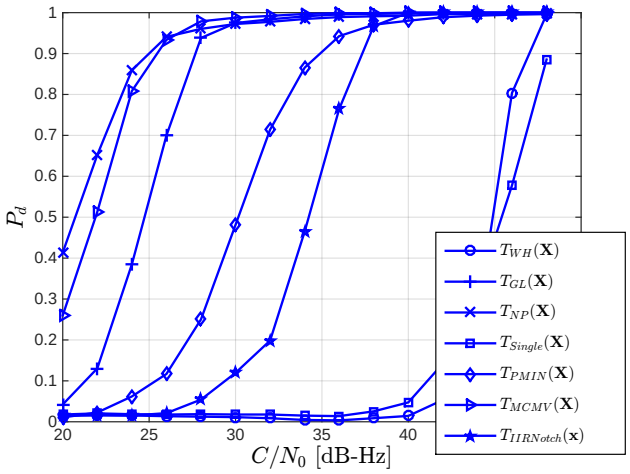

Fig. 5. Probability of detection P_d vs. satellite signal's C/N_0 with a 500 kHz wideband interference impinging into the receiver with $J/N_0 = 80$ dB-Hz. The acquisition threshold was configured for a constant probability of false alarm $P_{\text{fa}} = 0.001$.

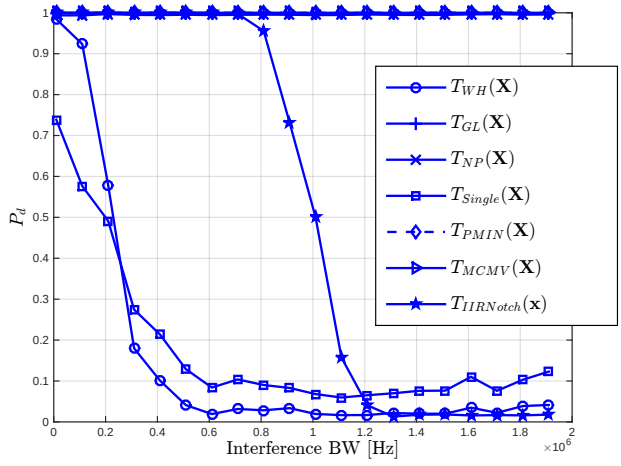

Fig. 6. Acquisition P_d vs. interference bandwidth impinging into the receiver with $J/N_0 = 80$ dB-Hz and constant satellite signal $C/N_0 = 42$ dB-Hz, for several acquisition algorithms. The acquisition threshold was configured for a constant probability of false alarm $P_{\text{fa}} = 0.001$.

2) Signal tracking performance: Beamformers' performance in signal tracking (*i.e.*, when estimations of time delay τ, carrier phase and Doppler shift are available) in the presence of an in–band, continuous wave jammer at 1.625 MHz from the central frequency was measured in an scenario where the desired signal came from a direction of arrival of 0^o in azimuth and 40^o in elevation with a carrier–to–noise density ratio of $C/N_0 = 35$ dB-Hz, and the interference came from an azimuth of 50^o and an elevation of 40^o.

The number of bits to be used for sample quantization at each of the receiver's digital stages are important design parameters, since they have a direct impact in the arithmetic computation architecture and the achieved performance [107]. Results of the signal-to-noise-plus-interference power ratio (SNIR) at the beamformers output are shown in Figure 7. It can be observed that the different algorithms improve performance until a certain number of bits are used, which then reach a plateau. In order to prevent from saturation, it was assumed an automatic gain control (AGC) at the input of the ADC that attenuates equally the incoming signal of all channels when the most significant bit of the ADC of reference is active. Interference power was set according to $J/N_0 = 80$ dB-Hz. Results were obtained by implementing fixed–point arithmetics for the downconversion and decimation stages, with a digital AGC that kept the most significant bits, as well as for the complex beamweight multiplier and the final channels' combination.

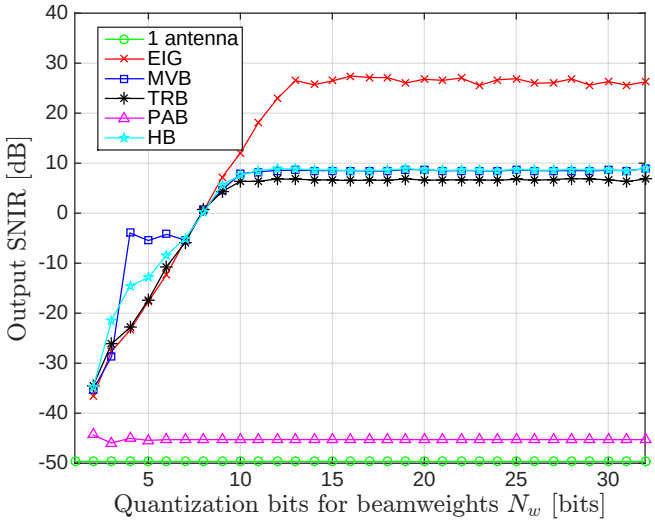

Fig. 7. Assessment of bit-length impact in weight quantization.

Results in Figure 8, averaging over 100 independent realizations, show the SNIR before and after beamforming. Simulations took into account a mismatch of 5^o between the estimated spatial signature vector $\hat{\mathbf{h}}_0$ and the actual one, $\mathbf{h}_0$, both in azimuth and elevation. Inaccuracies in the synchronization parameters were considered as well: half of the chip period in the time delay and ± 250 Hz in the Doppler shift of the reference $\mathbf{d}_0$, and ± 2 dB of error in the estimation of $|a_0|^2$. The spatio-temporal elements of $\mathbf{X}$ were quantized with 12 bits, and the resolution of the beamweights set to 16 bits.

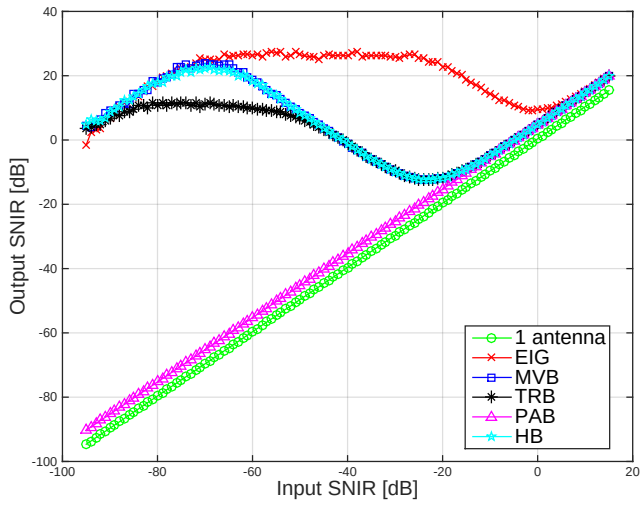

Fig. 8. SNIR before and after beamforming.

3) Multipath mitigation: In order to consider the effects of multipath (that is, $M(m) \neq 0$ in model (7)), the scenario consisted of an array with the same setup than in previous experiments, one Galileo E1 signal with an elevation of 45^o and an azimuth of 180^o received at $C/N_0 = 35$ dB-Hz, and a close replica spaced in time 0.25 chip period with respect to the line of sight signal, and with a power 3 dB below it. The echo impinged the array also with an elevation of 45^o and swept all the azimuth angle range. Figure 9 shows the rejection provided by different beamformers depending on the azimuth separation between the line of sight and the echo, averaged over 200 independent iterations.

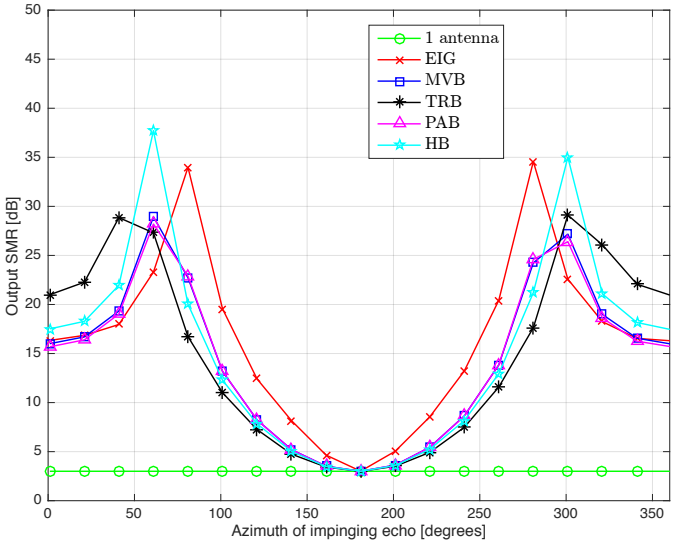

Fig. 9. Signal to multipath ratio (SMR) at the output of different beamformers in the presence of an echo 3 dB below the line of sight.

As expected, temporal-based methods exhibited poorer multipath rejection capabilities than those based on the direction of arrival. Again, the eigenbeamformer performed slightly better that other alternatives, specially when the line of sight and the echo came from directions of arrival close to each other. The error in DOA estimation was modeled as a Gaussian additive error term with a mean value of $\mu_e = 0°$ and variance $\sigma_e^2 = 10°$, and $\mu_e = 20°$) in both azimuth and elevation angles.

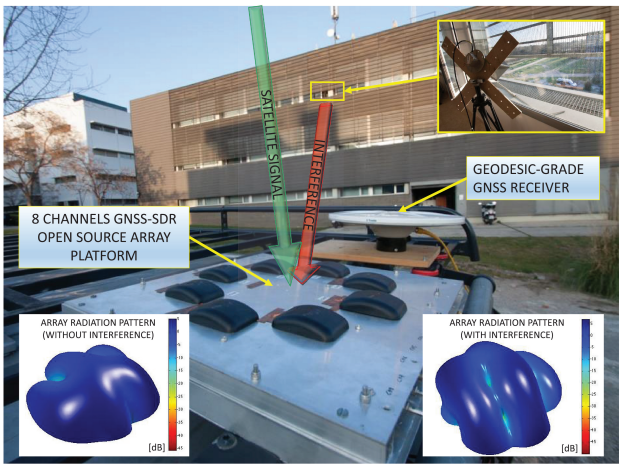

Fig. 10. Image of the experimental setup for interference robustness assessment with real-life signals.

B. Real–life experiments

The effective protection against strong interferences when using real-life signals was put under test by means of the physical implementation of an antenna array. The prototype was an arrangement of 8 antenna elements, in a circular geometry and spaced half a wavelength from each other. Each antenna element was followed by a radio-frequency front end, and all the downconverted outputs were digitized using a single, multiport ADC that ensured sampling coherence among channels. The eight digital streams were then connected to a FPGA device in charge of capturing matrix $\mathbf{X}$, computing the weights and applying them to the data stream, thus delivering a single output that fed a software-defined radio GNSS receiver in charge of performing all the baseband processing. Details of the implementation can be found in [108], and a picture of the experiment is shown in Figure 10.

The performance of the prototype was tested in harsh interference environment conditions. The receiver was located in an open-sky scenario where a strong uncorrelated in-band jammer impinged into the array with controllable direction of arrival and power. The interference was transmitted using an auxiliary directive antenna with a DOA of $\theta = 45^o$ and $\phi = 45^o$ with respect to the antenna platform. The satellite signal power and the interference (or jammer) power were measured in terms of C/N_0 and J/N_0, respectively. The C/N_0 was measured using the output of the receiver's correlators during signal tracking, whereas the J/N_0 was measured at the outputs of the front-ends. The AGC function was turned off and the front-end was configured at a maximum gain. During the experiment, the receiver acquired and tracked a near-zenithal GPS satellite in the presence of the jammer.

The interference protection offered by the implemented array was tested by performing a sweep of the interference power while trying to acquire and track a visible GPS satellite

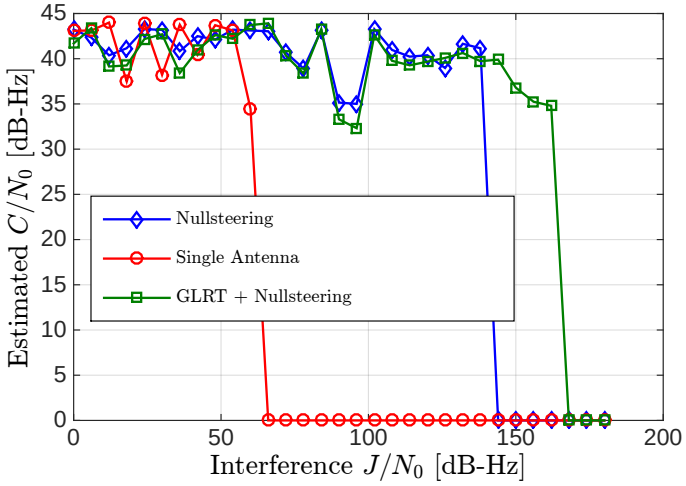

Fig. 11. Results of the interference robustness assessment with real-life signals.

signal. The interference J/N_0 sweep started at 0 dB-Hz and ended at 180 dB-Hz, which represents a high-power jammer nearby the GNSS receiver. The software receiver ran in real-time and captured 10 seconds of the C/N_0 estimations provided by the receiver's tracking loops. The receiver was configured to deliver an output each millisecond, so $10,000$ observations for each interference power level were recorded. Figure 11 shows the averaged results.

The single antenna receiver, without any time or frequency domain interference protection, was able to track the satellite signal until the interference power overtook the despreading gain, which for GPS L1 C/A signals is approximately 30 dB. This situation happened at $J/N_0 = 50$ dB-Hz. In contrast, the power minimization nuller provided an excellent interference protection, since the receiver was able to acquire and track the satellite signal until the interference power reached $J/N_0 = 90$ dB-Hz. Finally, enabling the GLRT-based acquisition of Section III-C, an extra protection of 10 dB was obtained due to the ability of the algorithm to point the array towards the satellite by computing $\mathbf{r}_{xd}$. Results in Figure 11 show that the extra anti-jamming protection provided by the antenna array can reach up to 100 dB, thus demonstrating its effectiveness.

VI. Conclusions

Controlled radiation pattern antennas constitute a powerful tool for multipath and interference rejection, thus increasing the accuracy, availability and reliability of the GNSS receiver. Depending on the information available at the antenna and the computational power, several receiver array architectures and signal processing techniques are possible. This paper presented an overview of the options, their trade-offs, implementation challenges and technology trends for the deployment of robust, satellite-based, navigation receivers. A plethora of combinations exist, being the final design based on the requirements imposed by the specific application at hand. The article concludes with some configuration examples, including experimental results using a specific implementation on a prototype.

Acknowledgment

This work has been partially supported by the Spanish Ministry of Economy and Competitiveness through project TEC2015-69868-C2-2-R (ADVENTURE) and by the Government of Catalonia under Grant 2014–SGR–1567.

References

[1] D. Dardari, P. Closas, and P. Djuric, "Indoor tracking: Theory, methods, and technologies," *IEEE Trans. Veh. Technol.*, vol. 64, no. 4, pp. 1263–1278, Apr. 2015. DOI: 10.1109/TVT.2015.2403868

[2] M. Hernández–Pajares, J. Miguel Juan, J. Sanz, A. Aragón–Ángel, P. Ramos Bosch, J. Samson, M. Tossaint, M. Albertazzi, D. Odijk, P. J. G. Teunissen, P. de Bakker, S. Verhagen, and H. van der Marel, "Wide–Area RTK. High precision positioning on a continental scale," *Inside GNSS*, vol. 5, no. 2, pp. 35–46, Mar./Apr. 2010.

[3] M. Thomas, *Global Navigation Space Systems: reliance and vulnerabilities*. London, UK: The Royal Academy of Engineering, Mar. 2011, ISBN 1-903496-62-4.

[4] F. Dovis, Ed., *GNSS Interference Threats and Countermeasures*. Norwood, MA: Artech House, 2015.

[5] B. Motella, M. Pini, and F. Dovis, "Investigation on the effect of strong out–of–band signals on global navigation satellite systems receivers," *GPS Solutions*, vol. 12, no. 2, pp. 77–86, Mar. 2008. DOI: 10.1007/s10291-007-0085-5

[6] I. Ilie, R. J. Landry, and M.-A. Fortin, *Real–World Interference Impacts Analysis using High Dynamic Range GNSS RF/IF Signals Record and Playback*. Montreal, Canada: Averna Technologies Inc., Oct. 2009.

[7] M. Kayton and W. R. Fried, *Avionics Navigation Systems*, 2nd ed. Hoboken, NJ: John Wiley & Sons, Inc., Apr. 1997.

[8] W. R. Vincent, R. W. Adler, P. McGill, J. R. Clynch, G. Badger, and A. A. Parker, "The hunt for RFI: unjamming a coast harbor," *GPS World*, vol. 14, no. 1, pp. 16–23, Jan. 2003.

[9] G. Xingxin Gao, L. Heng, A. Hornbostel, H. Denks, M. Meurer, T. Walter, and P. Enge, "DME/TACAN interference mitigation for GNSS: algorithms and flight test results," *GPS Solutions*, vol. 17, no. 4, pp. 561–573, Oct. 2013. DOI: 10.1007/s10291-012-0301-9

[10] RTCA, Inc., "DO–292, Assessment of radio frequency interference relevant to the GNSS L5/E5A frequency band," Washington, DC, July 2004.

[11] Electronic Communications Committee, "ECC Report 90. Compatibility of wind profile radars in the radiolocation service (RLS) with the radionavigation satellite service (RNSS) in the band 1270–1295 MHz," Lübeck, Germany, Sep. 2006.

[12] P. W. Ward, J. W. Betz, and C. J. Hegarty, "Interference, multipath, and scintillation," in *Understanding GPS. Principles and Applications*, 2nd ed., E. D. Kaplan and C. J. Hegarty, Eds. Norwood, MA: Artech House, 2006, pp. 243–299.

[13] A. T. Balaei, A. G. Dempster, and L. Lo Presti, "Characterization of the effects of CW and pulse CW interference on the GPS signal quality," *IEEE Trans. Aerosp. Electron. Syst.*, vol. 45, no. 4, pp. 1418–1431, Oct. 2009. DOI: 10.1109/TAES.2009.5310308

[14] P. W. Ward, "GNSS robustness: The interference challenge," in *Proc. 23rd Int. Tech. Meeting Sat. Div. Inst. Navig.*, Fort Worth, TX, Sep. 2010, pp. 69–97.

[15] U.S. National PNT Advisory Board, "Comments on jamming the Global Positioning System - A national security threat: Recent events and potential cures," Nov. 2010, White Paper.

[16] J. S. Warner and R. S. Johnston, "A simple demonstration that the global positioning system (GPS) is vulnerable to spoofing," *J. Security Administration*, vol. 25, no. 2, pp. 19–27, 2002.

[17] J.-C. Juang, "Analysis of Global Navigation Satellite System position deviation under spoofing," *IET Radar Sonar Navig.*, vol. 3, no. 1, pp. 1–7, Feb. 2009. DOI: 10.1049/iet-rsn:20070153

[18] D. P. Shepard, T. E. Humphreys, and A. A. Fansler, "Evaluation of the vulnerability of Phasor Measurement Units to GPS spoofing attacks," *International Journal of Critical Infrastructure Protection*, vol. 5, no. 3-4, pp. 146–153, Dec. 2012. DOI: 10.1016/j.ijcip.2012.09.003

[19] A. J. Kerns, D. P. Shepard, J. A. Bhattia, and T. E. Humphreys, "Unmanned aircraft capture and control via GPS spoofing," *J. Field Robotics*, vol. 31, no. 4, pp. 617–636, Jul./Aug. 2014. DOI: 10.1002/rob.21513

[20] E. G. Manfredini, B. Motella, and F. Dovis, "Signal quality monitoring for discrimination between spoofing and environmental effects inducing correlation," in *Proc. 28th Intl. Tech. Meeting Sat. Div. Inst. Navig.*, Tampa, FL, Sept. 2015, pp. 3100–3106.

[21] J. Magiera and R. Katulski, "Detection and mitigation of GPS spoofing based on antenna array processing," *J. Applied Research Technology*, vol. 13, no. 1, pp. 45–57, Feb. 2015. DOI: 10.1016/S1665-6423(15)30004-3

[22] D. Borio, L. Camoriano, S. Savasta, and L. Lo Presti, "Time–frequency excision for GNSS applications," *IEEE Syst. J.*, vol. 2, no. 1, pp. 27–37, Mar. 2008. DOI: 10.1109/JSYST.2007.914914

[23] A. T. Balaei, B. Motella, and A. G. Dempster, "A preventative approach to mitigating CW interference in GPS receivers," *GPS Solutions*, vol. 12, no. 3, pp. 199–209, Jul. 2008. DOI: 10.1007/s10291-007-0082-8

[24] S. Savasta, L. Lo Presti, and M. Rao, "Interference mitigation in GNSS receivers by a time-frequency approach," *IEEE Trans. Aerosp. Electron. Syst.*, vol. 49, no. 1, pp. 415–438, Jan. 2013. DOI: 10.1109/TAES.2013.6404112

[25] A. Martineau, C. Macabiau, O. Julien, I. Nikiforov, and B. Roturier, "GPS/Galileo RAIM performance in presence of multiple pseudorange failures due to interference," in *Proc. 20th Int. Tech. Meeting Sat. Div. Inst. Navig.*, Fort Worth, TX, Sep. 2007, pp. 3045–3056.

[26] M. D. Zoltowski and A. S. Gecan, "Advanced adaptive null steering concepts for GPS," in *IEEE Military Commun. Conf.*, vol. 3, San Diego, CA, Nov. 1995. DOI: 10.1109/MILCOM.1995.483688 pp. 1214–1218.

[27] A. Gecan and M. Zoltowski, "Power minimization techniques for GPS null steering antenna," in *Proc. 8th Int. Tech. Meeting Sat. Div. Inst. Navig.*, Palm Strings, CA, Sep. 1995, pp. 861–868.

[28] R. L. Fante and J. J. Vaccaro, "Wideband cancellation of interference in a GPS receive array," *IEEE Trans. Aerosp. Electron. Syst.*, vol. 36, no. 2, pp. 549–564, Apr. 2000. DOI: 10.1109/7.845241

[29] Z. Fu, A. Hornbostel, J. Hammesfahr, and A. Konovaltsev, "Suppression of multipath and jamming signals by digital beamforming for GPS/Galileo applications," *GPS Solutions*, vol. 6, no. 4, pp. 257–264, Mar. 2003. DOI: 10.1007/s10291-002-0042-2

[30] G. Carrié, F. Vincent, T. Deloues, D. Pietin, and A. Renard, "A new blind adaptive antenna array for GNSS interference cancellation," in *Proc. 39th Asilomar Conf. Signals, Systems and Comput.*, Pacific Grove, CA, Oct. 28 - Nov. 1 2005. DOI: 10.1109/ACSSC.2005.1599978 pp. 1326–1330.

[31] G. Seco–Granados, J. Fernández–Rubio, and C. Fernández–Prades, "ML estimator and hybrid beamformer for multipath and interference mitigation in GNSS receivers," *IEEE Trans. Signal Process.*, vol. 53, no. 3, pp. 1194–208, Mar. 2005. DOI: 10.1109/TSP.2004.842193

[32] M. G. Amin and W. Sun, "A novel interference suppression scheme for global navigation satellite systems using antenna array," *IEEE J. Sel. Areas Commun.*, vol. 23, no. 5, pp. 999–1012, May 2005.

[33] S. Kalyanaraman and M. Braasch, "Phase compensation in GPS array processing using a software radio," in *Proc. of the IEEE/ION Position, Location, And Navigation Symposium*, San Diego, CA, Apr. 2006. DOI: 10.1109/PLANS.2006.1650619 pp. 324–334.

[34] M. Sahmoudi and M. Amin, "Optimal robust beamforming for interference and multipath mitigation in GNSS arrays," in *Proc. IEEE Int. Conf. Acoust. Speech Signal Process.*, vol. 3, Honolulu, HI, Apr. 2007. DOI: 10.1109/ICASSP.2007.366774 pp. 693–696.

[35] A. J. O'Brien and I. J. Gupta, "Comparison of output SINR and receiver C/N_0 for GNSS adaptive antennas," *IEEE Trans. Aerosp. Electron. Syst.*, vol. 45, no. 4, pp. 1630–1640, Oct. 2009. DOI: 10.1109/TAES.2009.5310324

[36] S. Rougerie, C. G., F. Vincent, L. Ries, and M. Monnerat, "A new multipath mitigation method for GNSS receivers based on antenna array," *Intl. J. Navigation Observation*, vol. 2012, Article ID 804732, 2012. DOI: 10.1155/2012/804732

[37] H. Keshvadi, A. Broumandan, and G. Lachapelle, "Spatial characterization of GNSS multipath channels," *Intl. J. Antennas Propagation*, vol. 2012, Article ID 236464, 2012. DOI: 10.1155/2012/236464

[38] J. Arribas, P. Closas, C. Fernández-Prades, M. Cuntz, A. Konovaltsev, and M. Meurer, "Advances in the theory and implementation of GNSS antenna array receivers," in *Microwave and Millimeter Wave Circuits and Systems: Emerging Design, Technologies and Applications*, A. Georgiadis, H. Rogier, L. Roselli, and P. Arcioni, Eds. Chichester, UK: Wiley, 2012, pp. 227–273.

[39] P. J. G. Teunissen, "A-PPP: Array-aided precise point positioning with global navigation satellite systems," *IEEE Trans. Signal Process.*, vol. 60, no. 6, pp. 2870–2881, Jun. 2012. DOI: 10.1109/TSP.2012.2189854

[40] B. Li and P. J. G. Teunissen, "GNSS antenna array-aided CORS ambiguity resolution," *J. Geodesy*, vol. 88, no. 4, pp. 363–376, Apr. 2014. DOI: 10.1007/s00190-013-0688-2

[41] P. Stoica and M. Viberg, "Maximum likelihood parameter and rank estimation in reduced–rank multivariate linear regressions," *IEEE Trans. Signal Process.*, vol. 44, no. 12, pp. 3069–3078, Dec. 1996. DOI: 10.1109/78.553480

[42] M. Zatman, "How narrow is narrowband?" in *Proc. 31st Asilomar Conf. Sig., Syst., Comp.*, Pacific Grove, CA, Sep. 1997. DOI: 10.1109/ACSSC.1997.679122 pp. 2491–2498.

[43] C. Fernández-Prades, L. Lo Presti, and E. Falleti, "Satellite radiolocalization from GPS to GNSS and beyond: Novel technologies and applications for civil mass-market," *Proc. IEEE*, vol. 99, no. 11, pp. 1882–1904, Nov. 2011. DOI: 10.1109/JPROC.2011.2158032

[44] W. Kunysz, "A three dimensional choke ring ground plane antenna," in *Proc. 16th Intl. Tech. Meeting Inst. Navig.*, Portland, OR, Sep. 2003, pp. 1883–1888.

[45] M. Abdizadeh, J. T. Curran, and G. Lachapelle, "Quantization effects in GNSS receivers in the presence of interference," in *Proc. Intl. Tech. Meeting Inst. Navig.*, Newport Beach, CA, Jan. 2012, pp. 742–779.

[46] S. Gunawardena, J. Dickman, and M. A. Cosgrove, "Systems and methods for adaptive sample quantization," Patent US 8 923 414 B2, Dec. 30, 2014.

[47] F. Bastide, D. Akos, C. Macabiau, and B. Roturier, "Automatic gain control (AGC) as an interference assessment tool," in *Proc. 16th Int. Tech. Meeting Sat. Div. Inst. Navig.*, Porland, OR, Sep. 2003, pp. 2042–2053.

[48] D. Borio and E. Cano, "Optimal Global Navigation Satellite System pulse blanking in the presence of signal quantisation," *IET Signal Process.*, vol. 7, no. 5, pp. 400–410, Jul. 2013. DOI: 10.1049/iet-spr.2012.0199

[49] Y. R. Chien, "Design of GPS anti-jamming systems using adaptive notch filters," *IEEE Syst. J.*, vol. 9, no. 2, pp. 451–460, June 2015. DOI: 10.1109/JSYST.2013.2283753

[50] M. Sahmoudi and M. G. Amin, "Robust tracking of weak GPS signals in multipath and jamming environments," *Signal Processing*, vol. 89, no. 7, pp. 1320–1333, Jul. 2009. DOI: 10.1016/j.sigpro.2009.01.001

[51] D. Gustafson, J. Dowdle, J. Elwell, and K. Flueckiger, "A nonlinear code tracking filter for GPS-based navigation," *IEEE J. Sel. Topics Signal Process.*, vol. 3, no. 4, pp. 627–638, Aug. 2009. DOI: 10.1109/JSTSP.2009.2024590

[52] K. D. Wesson, B. L. Evans, and T. E. Humphreys, "A combined symmetric difference and power monitoring GNSS anti-spoofing technique," in *Proc. IEEE Global Conf. Signal Information Process.*, Austin, TX, 2013. DOI: 10.1109/GlobalSIP.2013.6736854 pp. 217–220.

[53] A. Jafarnia-Jahromi, A. Broumandan, J. Nielsen, and G. Lachapelle, "GPS vulnerability to spoofing threats and a review of antispoofing techniques," *Intl. J. Navigation and Observation*, vol. 2012, Article ID 127072, 2012. DOI: 10.1155/2012/127072

[54] G. A. McGraw, "Toughening GPS receivers against interference. Ensuring signal reception in spectrally busy environments," Rockwell Collins, Tech. Rep., Dec. 2014.

[55] O. L. Frost, III, "An algorithm for linearly constrained adaptive array processing," *Proc. IEEE*, vol. 60, no. 8, pp. 926–935, Aug. 1972. DOI: 10.1109/PROC.1972.8817

[56] F. G. Hatke, "Adaptive array processing for wideband nulling in GPS systems," in *Proc. 32th Asilomar Conf. Signals, Systems, & Comput.*, vol. 2, Pacific Grove, CA, Nov. 1998. DOI: 10.1109/ACSSC.1998.751542 pp. 1332–1336.

[57] S.-J. Kim and R. A. Iltis, "STAP for GPS receiver synchronization," *IEEE Trans. Aerosp. Electron. Syst.*, vol. 40, no. 1, pp. 132–144, Jan. 2004. DOI: 10.1109/TAES.2004.1292148

[58] D. S. De Lorenzo, "Navigation accuracy and interference rejection for GPS adaptive antenna arrays," Ph.D. dissertation, Dept. Aeronautics and Astronautics, Stanford University, Aug. 2007.

[59] R. Ebrahimi and S. R. Seydnejad, "Elimination of pre-steering delays in space-time broadband beamforming using frequency domain constraints," *IEEE Commun. Lett.*, vol. 17, no. 4, pp. 769–772, Apr. 2013. DOI: 10.1109/LCOMM.2013.022713.130090

[60] U.S. Air Force, "Advanced digital antenna production system," Harlow, UK, Mar. 2014, Fact Sheet.

[61] Novatel, Inc., "Single-enclosure GPS anti-jam technology (GAJT®)," Calgary, Canada, August 2015, GAJT-710ML Product Sheet.

[62] R. A. Qamar and N. M. Khan, "Null steering, a comparative analysis," in *Proc. IEEE 13th Intl. Multitopic Conf.*, Islamabad, Pakistan, Dec. 2009. DOI: 10.1109/INMIC.2009.5383130 pp. 1–5.

[63] M. Li, A. G. Dempster, A. T. Balaei, C. Rizos, and F. Wang, "Switchable beam steering/null steering algorithm for CW interference mitigation in GPS C/A code receivers," *IEEE Trans. Aerosp. Electron. Syst.*, vol. 47, no. 3, pp. 1564–1579, Jul. 2011. DOI: 10.1109/TAES.2011.5937250

[64] S. Mehmood, Z. Ullah Khan, F. Zaman, and B. Shoaib, "Performance analysis of the different null steering techniques in the field of adaptive beamforming," *Research J. Applied Sciences, Engineering and Technology*, vol. 5, no. 15, pp. 4006–4012, Apr. 2013.

[65] J. T. Curran, M. Bavaro, and J. Fortuny, "A comparison of analog and digital nulling techniques for multi-element antennas in GNSS receivers," in *Proc. 28th Intl. Tech. Meeting Inst. Navig.*, Tampa, FL, Sep. 2015, pp. 3249–3261.

[66] S. P. Applebaum, "Adaptive arrays," *IEEE Trans. Antennas Propag.*, vol. 24, no. 5, pp. 585–598, Sep. 1976. DOI: 10.1109/TAP.1976.1141417

[67] B. Widrow, P. E. Mantey, L. J. Griffiths, and B. B. Goode, "Adaptive antenna systems," *Proc. IEEE*, vol. 55, no. 12, pp. 2143–2159, Dec. 1967. DOI: 10.1109/PROC.1967.6092

[68] B. Allen and M. Ghavami, *Adaptive Array Systems: Fundamentals and Applications*. Norwood, MA: Wiley, 2015.

[69] M. Cuntz, A. Konovaltsev, A. Hornbostel, E. Schittler Neves, and A. Dreher, "GALANT - Galileo antenna and receiver demonstrator for safety-critical applications," in *Proc. 10th European Conf. Wireless Technology*, Munich, Germany, Oct. 2007, pp. 59–61.

[70] M. Sgammini, F. Antreich, L. Kurz, M. Meurer, and T. G. Noll, "Blind adaptive beamformer based on orthogonal projections for GNSS," in *Proc. 25th Int. Tech. Meeting Sat. Div. Inst. Navig.*, Nashville, TN, Sep. 2012, pp. 926–935.

[71] M. Mañosas-Caballú, G. Seco-Granados, and A. L. Swindlehurst, "Robust beamforming via FIR filtering for GNSS multipath mitigation," in *Proc. IEEE Intl. Conf. Acoust., Speech, Signal Process.*, Vancouver, BC, May 2013. DOI: 10.1109/ICASSP.2013.6638445 pp. 4173–4177.

[72] NAVSYS Corporation, "High gain advanced GPS receiver. White paper," Colorado Springs, CO, Sep. 2002.

[73] A. Konovaltsev, F. Antreich, and A. Hornbostel, "Performance assessment of antenna array algorithms for multipath and interference mitigation," in *Proc. 2nd Workshop GNSS Signals & Signal Process.*, ESTEC, Noordwijk, The Netherlands, 2007. [Online]. Available: http://elib.dlr.de/48991/

[74] J. Liu, B. Weaver, Y. Zakharov, and G. White, "An FPGA-based MVDR beamformer using dichotomous coordinate descent iterations," in *Proc. IEEE Int. Conf. Commun.*, Glasgow, Scotland, June 2007. DOI: 10.1109/ICC.2007.422 pp. 2551–2556.

[75] M. Li, F. Wang, A. Tabatabei, A. G. Dempster, and C. Rizos, "A novel beamforming architecture with software GNSS receiver implementation," in *Proc. Intl. Symp. GPS/GNSS*, Yokohama, Japan, Nov. 2008, pp. 904–909.

[76] Y.-H. Chen, J.-C. Juang, J. Seo, S. Lo, D. M. Akos, D. S. De Lorenzo, and P. Enge, "Design and implementation of real-time software radio for anti-interference GPS/WAAS sensors," *Sensors*, vol. 12, no. 10, pp. 13 417–13 440, Oct. 2012. DOI: 10.3390/s121013417

[77] S. Daneshmand, "GNSS interference mitigation using antenna array processing," Ph.D. dissertation, Department of Geomatics Engineering, University of Calgary, Apr. 2013.

[78] F. Chan, J. Choi, and J. Wang, "A robust signal acquisition and tracking architecture with ultra-tight integration of GPS/INS/PL and multiple antenna array," in *Proc. Intl. Symp. GPS/GNSS*, Hong Kong, Dec. 2005, pp. 1–9.

[79] M. Lu, J. Wang, R. Babu, D. Li, and Z. Feng, "A novel antenna array for GPS/INS/PL integration," *J. of GPS*, vol. 4, no. 1–2, pp. 160–165, 2005. DOI: 10.5081/jgps.4.1.160

[80] M. Moore, C. Rizos, and J. Wang, "Quality control issues relating to an attitude determination system using a multi-antenna GPS array," *Geomatics Research Australasia*, vol. 77, pp. 27–48, Dec. 2002.

[81] A. T. Balaei and A. G. Dempster, "Phase calibration and attitude determination of a 2 by 2 phased array GNSS antenna," in *Proc. Intl. Symp. GPS/GNSS*, Yokohama, Japan, Nov. 2008, pp. 983–989.

[82] R. J. Mailloux, *Phased Array Antenna Handbook*. Norwood, MA: Artech House, Inc., 2005.

[83] Z. U. Khan, A. Naveed, I. M. Qureshi, and F. Zaman, "Independent null steering by decoupling complex weights," *IEICE Electron. Express*, vol. 8, no. 13, pp. 1008–1013, July 2011. DOI: 10.1587/elex.8.1008

[84] D. Turbiner, "Phased antenna array for global navigation satellite system signals," Patent US 20 130 342 397 A1, Dec. 26, 2013.

[85] R. G. Lorenz and S. P. Boyd, "Robust minimum variance beamformer," in *Robust Adaptive Beamforming*, J. Li and P. Stoica, Eds. Hoboken, NJ: John Wiley & Sons, Inc., 2006, ch. 1, pp. 1–46.

[86] R. A. Monzingo and T. W. Miller, *Introduction to Adaptive Arrays*. Raleigh, NC: Scitech Publishing, Inc., 2004.

[87] C. Fernández-Prades, P. Closas, and J. Arribas, "Eigenbeamforming for interference mitigation in GNSS receivers," in *Proc. Intl. Conf. Localization and GNSS*, Tampere, Finland, June 2011. DOI: 10.1109/ICL-GNSS.2011.5955267 pp. 93–97.

[88] S. M. Kay, *Fundamentals of statistical signal processing: Detection theory*. Upper Saddle River, NJ: Prentice Hall, 1998.

[89] J. Arribas, C. Fernández-Prades, and P. Closas, "Multi-antenna techniques for interference mitigation in GNSS signal acquisition," *EURASIP J. Adv. Signal Process.*, vol. 2013, no. 143, Sep. 2013. DOI: 10.1186/1687-6180-2013-143

[90] J. Arribas, P. Closas, and C. Fernández-Prades, "Interference mitigation in GNSS receivers by array signal processing: A software radio approach," in *Proc. IEEE 8th Sensor Array Multichannel Signal Process.*, A Coruña, Spain, June 2014. DOI: 10.1109/SAM.2014.6882355 pp. 121–124.

[91] A. Konovaltsev, L. Greda, M. V. T. Heckler, and A. Hornbostel, "Phase center variations in adaptive GNSS antenna arrays," in *Proc. 4th ESA Workshop on Satellite Navig. User Equipment Technol.*, Noordwijk, The Netherlands, Dec. 2008, pp. 1–8.

[92] H. Zhao, B. Lian, and J. Feng, "Adaptive beamforming and phase bias compensation for GNSS receiver," *J. of Syst. Eng. Electron.*, vol. 26, no. 1, pp. 10–18, Feb. 2015. DOI: 10.1109/JSEE.2015.00002

[93] C. L. Chang and J. C. Juang, "A new pre-processing approach against array uncertainty for GNSS," in *Proc. IEEE/ION Position, Location and Navig. Symp.*, vol. 16, Monterey, CA, May 2008. DOI: 10.1109/PLANS.2008.4569997 pp. 892–897.

[94] A. Konovaltsev, M. Cuntz, L. Greda, M. Heckler, and M. Meurer, "Antenna and RF front end calibration in a GNSS array receiver," in *Proc. IEEE Intl. Microwave Workshop Series on RF Front-ends for Software Defined and Cognitive Radio Solutions*, Aveiro, Portugal, Feb. 2010. DOI: 10.1109/IMWS.2010.5440984 pp. 103–106.

[95] A. J. 0'Brien and I. J. Gupta, "Mitigation of adaptive antenna induced bias errors in GNSS receivers," *IEEE Trans. Aerosp. Electron. Syst.*, vol. 47, no. 1, pp. 524–538, Jan. 2011. DOI: 10.1109/TAES.2011.5705689

[96] B. R. Rao, J. H. Williams, C. D. Boschen, J. T. Ross, E. N. Rosario, and R. J. Davis, "Characterizing the effects of mutual coupling on the performance of a miniaturized GPS adaptive antenna array," in *Proc. 13th Intl. Tech. Meeting Sat. Div. Inst. Navig.*, Salt Lake City, UT, Sep. 2000, pp. 2491–2498.

[97] E. Ngai and D. Blejer, "Mutual coupling analyses for small GPS adaptive arrays," in *IEEE Antennas Propag. Soc. Intl. Symp.*, vol. 4, Boston, MA, July 2001. DOI: 10.1109/APS.2001.959395 pp. 38–41.

[98] D. S. De Lorenzo, S. C. Lo, P. K. Enge, and J. Rife, "Calibrating adaptive antenna arrays for high-integrity GPS," *GPS Solutions*, vol. 16, no. 2, pp. 221–220, Apr. 2012. DOI: 10.1007/s10291-011-0224-x

[99] S. Daneshmand, N. Sokhandan, M. Zaeri-Amirani, and G. Lachapelle, "Precise calibration of a GNSS antenna array for adaptive beamforming applications," *Sensors*, vol. 14, no. 6, pp. 9669–9691, May 2014. DOI: 10.3390/s140609669

[100] J. A. Apolinário Jr., Ed., *QRD-RLS Adaptive Filtering*. New York, NY: Springer.

[101] Z. L. Yu, W. Se, and S. Rahadja, "QR-RLS based minimum variance distortionless responses beamformer," in *Proc. IEEE Intl. Conf. Acoust., Speech, Signal Process.*, vol. III, Toulouse, France, May 2006. DOI: 10.1109/ICASSP.2006.1660821 pp. 984–987.

[102] C. Dick, F. Harris, M. Pajic, and D. Vuletic, "Real-time QRD–based beamforming on an FPGA platform," in *Proc. 40th Asilomar Conf. Signals, Systems and Comput.*, Pacific Grove, CA, Nov. 2006. DOI: 10.1109/ACSSC.2006.354945 pp. 1200–1204.

[103] N. Lodha, N. Rai, R. Dubey, and H. Venkataraman, "Hardware-software co-design of QRD-RLS algorithm with Microblaze soft core processor," in *Proc. 3rd Intl. Conf. Inform. Syst. Technol. Manag.*, Ghaziabad, India, Mar. 2009. DOI: 10.1007/978-3-642-00405-6_23 pp. 197–207.

[104] L. T. Ong and B. Sarankumar, "QRD-based and SMI-based MVDR beamforming for GNSS software receivers," in *Proc. 26th Int. Tech. Meeting Sat. Div. Inst. Navig.*, Nashville, TN, Sep. 2013, pp. 3450–3455.

[105] European Union, *European GNSS (Galileo) Open Service. Signal In Space Interface Control Document. Ref: OS SIS ICD, Issue 1.2*, Brussels, Belgium, Nov. 2015.

[106] J. Arribas, C. Fernández-Prades, and P. Closas, "Antenna array based GNSS signal acquisition for interference mitigation," *IEEE Trans. Aerosp. Electron. Syst.*, vol. 49, no. 1, pp. 223–243, Jan. 2013. DOI: 10.1109/TAES.2013.6404100

[107] J. Betz and N. Shnidman, "Receiver processing losses with bandlimiting and one-bit sampling," in *Proc. 20th Int. Tech. Meeting Sat. Div. Inst. Navig.*, Fort Worth, TX, Sep. 2007, pp. 1244–1256.

[108] J. Arribas, "GNSS array-based acquisition: Theory and implementation," Ph.D. dissertation, Dept. of Signal Theory and Communications, Universitat Politècnica de Catalunya, Barcelona, Spain, July 2012.

Carles Fernández–Prades (S'02–M'06–SM'12) received the M.Sc. and Ph.D. (*cum laude*) degrees in electrical engineering from the Universitat Politècnica de Catalunya (UPC), Barcelona, Spain, in 2001 and 2006, respectively. In 2001, he joined the Department of Signal Theory and Communication at UPC as a Research Assistant, getting involved in European and National research projects both with technical and managerial duties. He also was Teaching Assistant in the field of Analog and Digital Communications (UPC 2001-2005). In 2006 he joined CTTC, where he currently holds a position as Senior Researcher and serves as Head of the Communications Systems Division. His primary areas of interest include signal processing, estimation theory and nonlinear Bayesian filtering, with applications in positioning, communications systems, software radio and the design of RF front-ends. He proudly served as Thesis advisor of works acknowledged by the European Association for Signal Processing (EURASIP) with the Best Ph.D. Thesis Award in 2014 and 2015.

Javier Arribas (Barcelona, 1980) obtained the B.Sc. degree and the M.Sc degree in Telecommunication Engineering from La Salle School of Engineering (Ramon Llull University), in 2002 and 2004 respectively. From January 2004 to September 2005 he worked as Teaching Assistant at the Signal theory and Communications Department. He currently collaborates as M.Sc and B.Sc Theses advisor, involved in the SalleSat Cubesat picosatellite development program as technical director.

From February 2005 to December 2007 he founded Nadir Mobile Systems Engineering Company and he worked as the Engineering section director.

In 2008 he was awarded the Ph.D fellowship of the Centre Tecnològic de Telecomunicacions de Catalunya (CTTC). He received his Ph.D degree on Signal Theory and Communications from the Technical University of Catalonia (UPC), Spain, in 2012. He is the recipient of the EURASIP Best PhD Thesis Award 2015 for his Thesis "GNSS Array-Based Acquisition: Theory and Implementation".

He currently serves as Senior Researcher at the Communications Systems Division at CTTC in the Statistical Inference for Navigation and Positioning Department, in the Communications Systems Division, where he coordinates the Digital Signal Processing lab (DSP lab) facilities and the GNSS-SDR testbed. His primary areas of interest are the GNSS receiver design, RF front-end design, array signal processing, signal estimation and detection theory, with applications to positioning and communications systems. He has extended experience in both Software Defined Receivers (SDR) and FPGA-based real-time systems design and development.

Pau Closas (S'04–M'10–SM'13) received the M.Sc. and Ph.D. in Electrical Engineering from the Universitat Politècnica de Catalunya (UPC) in 2003 and 2009, respectively. He also holds a M.Sc. degree in Advanced Mathematics and Mathematical Engineering from UPC since 2014. In 2003, he joined the Department of Signal Theory and Communications, UPC, as a Research Assistant. During 2008 he was Research Visitor at the Stony Brook University (SBU), New York, USA.

In September 2009 he joined the CTTC, where he currently holds a position as a Senior Researcher and Head of the Statistical Inference for Communications and Positioning Department. He has many years of experience in projects funded by the European Commission, Spanish and Catalan Governments, as well as the European Space Agency in both technical and managerial duties. His primary areas of interest include statistical and array signal processing, estimation and detection theory, Bayesian filtering, robustness analysis, and game theory, with applications to positioning systems, wireless communications, and mathematical biology.

Pau Closas is Senior Member of IEEE, ION, and EURASIP. He was involved in the organizing committees of EUSIPCO'11, IEEE IMWS'11, IEEE RFID-TA'11, European Wireless'14, IEEE SSP'16, and IEEE ICASSP'20 conferences. He is the recipient of the EURASIP Best PhD Thesis Award 2014 and the 9^{th} Duran Farell Award for Technology Research, both in recognition to his contributions to the field of signal processing for GNSS.